Numerical Simulation of Nacelle Flowfield for Counter-Rotating Open Rotor Propellers

Citation for the original published paper (version of record):

Silva, V., Silva, L., Tomita, J. et al (2017). Numerical Simulation of Nacelle Flowfield for
Counter-Rotating Open Rotor Propellers. International Society of Air-breathing Engines (ISABE)

N.B. When citing this work, cite the original published paper.

(article starts on next page)

Numerical Simulation of Nacelle Flowfield for Counter-Rotating Open Rotor Propellers

Vinícius Tavares Silva, Lucilene Moraes da Silva, Jesuino Takachi Tomita and Cleverson Bringhenti
viniciustasil@gmail.com
Aeronautics Institute of Technology
Turbomachines Department
São José dos Campos
Brazil

Tomas Grönstedt, Olivier Petit and Alexandre Capitao Patrao
Chalmers University of Technology
Department of Mechanics and Maritime Sciences
Gothenburg
Sweden

ABSTRACT

This paper summarizes the development of a tool for designing axisymmetric nacelles for counter-rotating open rotor (CROR) engines, based on predefined geometries, global input relations and one-dimensional perfect gas equations. A nacelle geometry was generated to match with the flight conditions and base dimensions of the Airbus AI-PX7 CROR propeller. Furthermore, the 3D turbulent flowfield around the nacelle was evaluated via Computational Fluid Dynamics (CFD) for four different angles of attack: 0°, 4°, 6° and 8°. The computations were performed for the nacelle without the propellers as a first analysis. The formation of shock waves, boundary layer separation and inlet flow distortion were the main parameters of the CFD study. The nacelle design was considered to be successful as a preliminary approach, since, even for the highest angle of attack, no critical conditions for the engine performance were detected.

Keywords: CFD; Nacelle; Counter-Rotating Open Rotor

NOMENCLATURE

ACARE	Advisory Council for Aeronautics Research in Europe
AoA	Angle of attack
CFD	Computational fluid dynamics
CROR	Counter-rotating open rotor
CST	Class shape transformations
MFP	Mass flow parameter
HTR	Hub-to-tip ratio
RANS	Reynolds averaged Navier-Stokes
BR	Bottom region
TR	Top region

Symbols

$\bar{p}_{t\infty}$	Mass-weighted average of free stream total pressure [Pa]
$\bar{p}_{tF}$	Mass-weighted average of total pressure at the fan [Pa]
D_h	Hub diameter [m]
D_{hl}	Highlight diameter [m]
D_m	Maximum forebody diameter [m]
L_i	Intake length [m]
L_p	Plug length [m]
L_d	Diffuser length [m]
L_n	NACA 1 profile length [m]
L_{tot}	Total length of nacelle [m]
$\dot{m}$	Mass flow rate [kg/s]
p_0	Total Pressure [kPa]
R_e	Exhaust radius [m]
R_f	Fan radius [m]
R_h	Hub radius [m]
R_{hl}	Highlight radius [m]
R_m	Maximum forebody radius [m]
R_p	Plug radius [m]
R_{th}	Throat radius [m]
T_0	Total temperature [K]
a	Lip length [m]
b	Lip height [m]
M	Mach number [-]
R	Gas constant $\left[\frac{kJ}{kg \cdot K}\right]$
γ	Specific heat ratio [-]
η	Total pressure recovery [-]

1.0   INTRODUCTION

The sudden increase in fuel prices and the growing concern about aircraft environmental impact have renewed the interest in propeller based engine concepts over the last 20 years. The Advisory Council for Aeronautics Research in Europe (ACARE) has declared the objectives for 2050, among which there is a cut of 75% CO_2 and 65% perceived noise emissions, considering the year 2000 as reference [1]. Therefore, due to its high propulsive efficiency, the counter-rotating open rotor (CROR) architecture has been targeted as a potential engine configuration to achieve drastic reductions in fuel consumption and emissions. CROR technologies are expected to attain up to 35% fuel savings as well as substantial noise cutbacks [2].

CROR nacelles are non-adaptive structures which have to supply flow for the engine under different flight conditions fulfilling several aerodynamic requirements with the same geometry. Cowls have to be designed aiming to avoid excessive drag and prohibitive conditions during cruise, such as boundary layer separations due to high pressure gradients on lip or shock waves formation due to flow acceleration around the forebody [3]. For

take-off and landing, the nacelle configuration also must be suitable to operate under high flow angles of attack without excessive loss of performance.

Unlike turbofan engines, which fan blades are ducted by the nacelle, the propeller of a CROR engine is in direct contact with the flowfield. The lowest possible distortion to the unducted fan should thus be considered, under different power settings. The rear mounted propeller configuration leads to a forebody diameter ratio (D_{hl}/D_m) far below conventional high-speed turbofan design experience, which is the major reason for its unconventional shape [4].

Cowl and inlet design methodologies, as well as flowfield studies around different nacelle configurations are quite documented in the open literature. ESDU reports presented both a method for estimating the loss in pressure recovery of axisymmetric intakes under subsonic flight conditions, based on one-dimensional equations with averaged measured flow parameters [5] and a methodology for estimating the drag of axisymmetric cowls with sharp trailing edges, at subsonic flight conditions and zero incidence angle [3]. Detailed studies about subsonic and supersonic intake aerodynamics and practical design can be found in [6-7], where pressure recovery, intake drag and flow separation are some of the subjects.

An axisymmetric long-ducted nacelle for mixed stream subsonic turbofan engines was designed and the turbulent flowfield around it was simulated by Takachi et al. [8], for two angles of attack. A study to estimate the drag characteristics of a nacelle airfoil was carried out by Sharanabasappa et al. [9], for various angles of attack. Chen et al. have performed a parametric study aiming to evaluate the aerodynamic characteristics of a nacelle intake into three categories: Mach distribution, flow recovery and distortion [10], in which a geometry modelling is described and the flowfield is simulated via CFD. An investigation of the aerodynamic performance of an adaptive turbofan-engine inlet was presented by Majić et al. [11], where numerical flowfield investigations were performed. The effect of morphing the nacelle inlet geometry on the absolute total pressure recovery was evaluated and results showed benefits in performance at different flight conditions.

Christie and Heidebrecht [12] presented a tool for creating aerodynamic geometries based on the class shape transformation (CST) curves method, which was used to develop parametric geometry definitions for cowls and intakes. CFD analysis have shown that despite simplicity of the method, the obtained shapes were very close to the expected for a final design. The development of parametric definitions for a generic turbofan nacelle was defined by Heidebrecht et al. [13], based on CST curves. The study of the flowfield around the nacelle has shown that the aerodynamic performance results were very similar to those of the existing designs. The CST method, based on fourth order Bernstein polynomials, was also used by Petruson [14], for designing and performing parametric CFD studies of 2D axisymmetric nacelles for ultra-high bypass turbofan engines.

The design and development of the General Electric UnDucted Fan counter-rotating turbofan engine was reported in [4], where brief information concerning the engine nacelle aerodynamic design is given. Some relations used in the design of the intake and nozzle are also exposed. A design procedure description of a counter-rotating ultra-high-bypass-fan is exposed in [15]. The first design consisted of an axisymmetric nacelle, an axi-asymmetric 3D geometry was obtained after a reiteration procedure, and the flowfield calculations were performed using the Euler method. Multidisciplinary design features were presented by Negulescu [2], for modern high speed subsonic counter-rotating propellers for commercial airplanes. Furthermore, the design of a CROR propeller was presented along with a steady-state and unsteady CFD analysis of the propeller aerodynamics. Patrao et al. [16] presented an optimization platform for high speed propellers applied to the Boxprop, an innovative configuration, developed by GKN, intended to be used in CROR engines. Moreover, optimal design candidates were evaluated using CFD.

As the interest in CROR engines is clearly increasing over the last years, the necessity of a preliminary tool for designing a nacelle designated to this type of configuration becomes evident. Therefore, the aim of this paper is to provide a first step on the design of CROR nacelles as well as evaluating the flowfield around a chosen geometry under different flight conditions.

2.0   METHODOLOGY

This section describes the methodology for the axisymmetric nacelle shape generation based on predefined geometries, global input relations and one-dimensional perfect gas equations. Moreover, the mesh generation methods and the CFD flowfield numerical simulation definitions are here also presented.

2.1   Nacelle geometry design

The base dimensions for the geometry design as well as the flight conditions were chosen to match with the Airbus AI-PX7 CROR propeller [2]. Thus, a propeller diameter of 4.2672m, a HTR of 0.35 and a rotor disk spacing of

0.22 were selected. The nacelle was designed to a Mach number of 0.75, an altitude of 10668m and for ISA condition. For both propellers, the chord on hub position is 0.4267m.

The performance prediction program, GTAnalysis, of the ITA Turbomachines Department, was used to simulate a CROR, with a generic propeller, and hence select an approximate mass flow to match with the AI-PX7 propeller design thrust on cruise conditions [2].

A MATLAB code was developed aiming to generate a 2D axisymmetric nacelle geometry for CROR engines, based on one-dimensional perfect gas equations, global input relations and predefined geometries. The nacelle is divided into three parts: the forebody, the midbody and the afterbody. The former consists of an inlet and an external cowl, the second is the region of the counter-rotating propellers and the later holds the nozzle and plug.

The engine inlet consists of a spinner, a fan face, a diffuser and a lip. The spinner is described by a parabolic equation, whereas the lip consists of an ellipse followed by a sinusoidal diffuser. The forebody cowl is composed of a NACA 1 profile followed by a curvature of linearly changing second derivative[1].

The propeller blades, although performing a substantial influence in the flow downstream of the forebody, are not yet included in the geometry. Therefore, the midbody is cylindrical, considering only the spacings for the blade rows. The afterbody consists of a nozzle, with linearly changing curvature, followed by a conical plug, smoothed just downstream of the nozzle.

The fan and nozzle annular areas are calculated on the mass flow parameter (MFP), given by Equation 1.

$$MFP = \frac{\dot{m}\sqrt{T_0}}{p_0 A} = \sqrt{\frac{\gamma}{R}} M \left(1 + \frac{\gamma - 1}{2} M^2\right)^{\frac{\gamma+1}{2(1-\gamma)}} \qquad (\quad 1\quad)$$

The core mass flow used for the engine sizing was 13.5kg/s and the Mach numbers on fan face and nozzle exit plane were 0.6 and 0.8, respectively.

Figure 1 shows the nacelle with the main geometric parameters and Table 1 shows the global input relations used to construct its shape for the flowfield simulations.
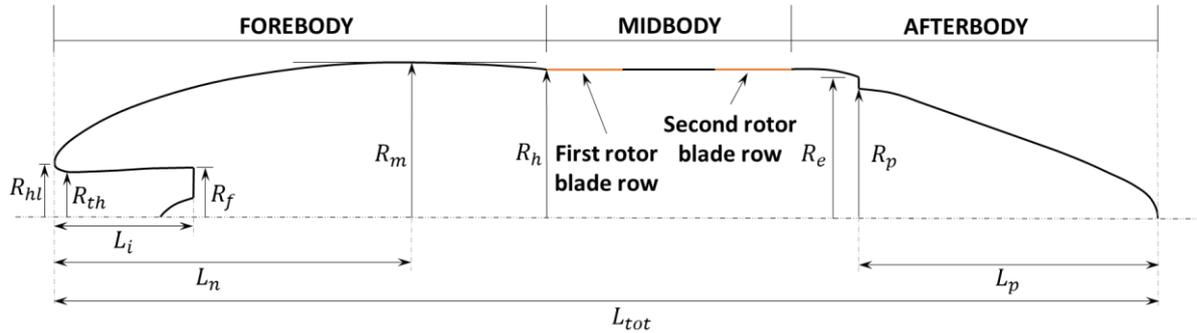

Figure 1 Nacelle shape with main geometric parameters.

Table 1
Global input relations for the nacelle geometry generation.

Relation	Value
L_d/D_f	1.30
R_{hl}^2/R_{th}^2	1.30
R_f/R_{th}	1.10
L_f/D_h	1.80
a/b	2.50
Fan HTR	0.40
L_n/D_h	1.15
R_{hl}/R_m	0.29
L_p/R_h	2.50

---

[1] The curve slope changes linearly, so that it starts tangentially to the NACA 1 profile and ends exactly in the first propeller beginning.

2.2 CFD simulations

Aiming to evaluate the suitability of the designed nacelle for an end of climb condition, four 3D CFD simulations were carried out, for angles of attack of 0°, 4°, 6° and 8°. The aim of the numerical calculations was to investigate the formation of shock waves, boundary-layer separation, deceleration of flow entering the engine, and intake flow distortion. The designed geometry was extracted to the commercial software ANSYS ICEM CFD, wherein an unstructured mesh with tetrahedral elements was generated. Prims layers were used on the nacelle surface, to generate thinner grids for boundary layer capturing. Moreover, the grid was transferred to the solver ANSYS Fluent 15 and the calculations were performed using the parallel computation technique, in a high-performance computer.

2.2.1 Mesh generation

The flow around the nacelle was simulated throughout an unstructured grid bounded by a farfield, consisting of a half sphere shell with $50R_m$ radius, followed by a cylindrical surface, as shown in Figure 2. The farfield length was chosen to be $50L_{tot}$ and the nacelle and farfield centroids were positioned at the same point.
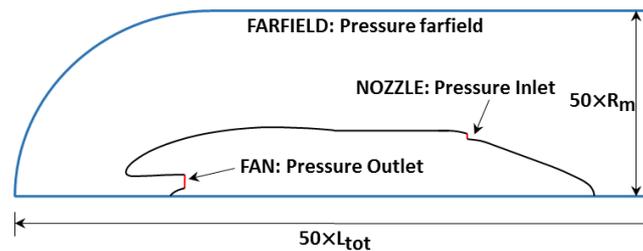
Figure 2 Farfield representation.

The use of wall functions is not recommended for the cases of boundary layer separation, which are likely to occur for the cases of AoA different than zero, hence resolving the viscous sublayer is necessary for the cases here studied, which demands a first grid cell of about $y^+ \approx 1$ [17]. These values could be obtained by the addition of prism layers on the nacelle surface.

To guarantee acceptable values of y^+, and a complete boundary capture by the prisms, as well as a smooth transition to the tetrahedral elements, a near wall treatment of 32 prism layers, with a height ratio of 1.25 was fulfilled in the intake, cowl and midbody surfaces. The final mesh used for the flowfield simulations consisted of about 11.6 million cells. The farfield and nacelle surface mesh are shown in Figure 3 and Figure 4 exhibits the volumetric mesh around the nacelle followed by a detail of the prism layers.

(a)   (b)
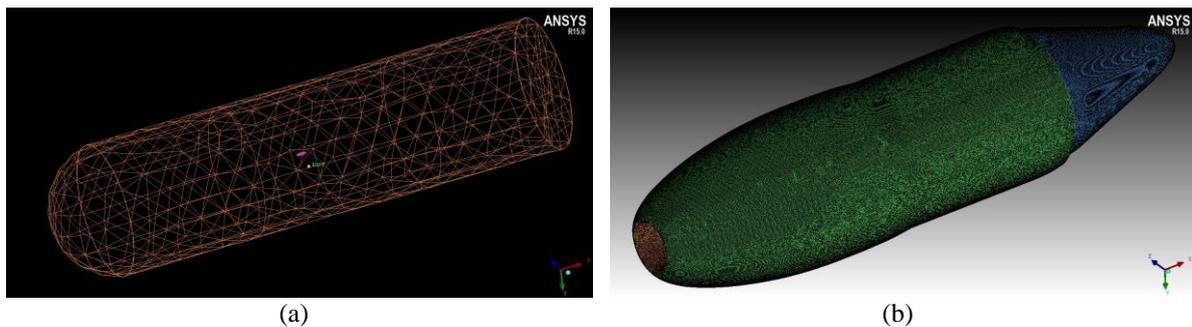
Figure 3 3D farfield surface mesh (a) and 3D nacelle surface mesh (b).
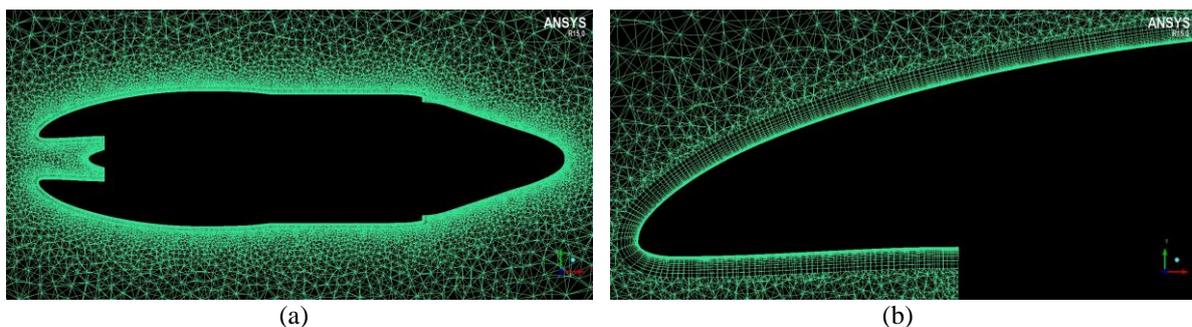

(a)   (b)

Figure 4 Unstructured volumetric mesh cut plane (a) and detail of the prism layers on the intake and cowl surfaces (b).

2.2.2   Mesh dependency study

A mesh dependence study was carried out to check the influence of the grid refinement on the solution. The selected parameter to perform the verification was the total pressure recovery η, defined by Equation 2.

$$\eta = \frac{\overline{p}_{tF}}{\overline{p}_{t\infty}}$$

(2)

Where $\overline{p}_{tF}$ is the mass-weighted average of total pressure at the fan and $\overline{p}_{t\infty}$ is mass-weighted average of free stream total pressure.

Five different mesh sizes were studied, ranging from a coarse mesh of nearly 700.000 cells to a fine mesh of about 11.6 million cells. The grid refinement was performed globally, by changing the maximum size of the surface elements. The grid convergence result is shown in Figure 5.
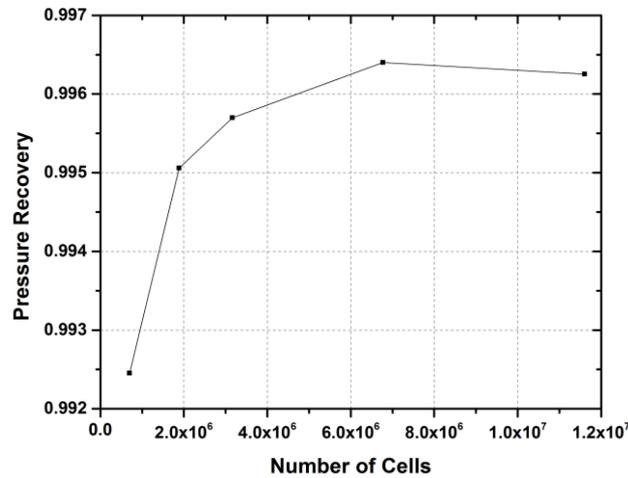
Figure 5 Mesh dependency study results.

The grid convergence was achieved for sizes above 6.76 million cells, since the error between the two finest grids is less than 0.015%. Nevertheless, the last tested mesh of 11.6 million of elements was selected for the simulations, due to a better orthogonal quality of prisms obtained for this size, resulting in better convergence of solutions.

2.2.3   CFD Solver settings

The 3D simulations were carried out using the Reynolds-Averaged Navier-Stokes equations, by applying the pressure-based solver together with the k-ω SST turbulence model. The pressure-velocity coupled scheme was selected jointly with third-order interpolations adopted for the convection terms and second-order upwind interpolations for the diffusive terms. Air was modelled as an ideal gas and viscosity was calculated using Sutherland's law, with the three coefficient equation.

The boundary conditions were settled in the farfield, fan face, and nozzle, as pressure farfield, pressure outlet and pressure inlet, respectively, as shown in Figure 2. The ambient pressure and temperature used in the pressure farfield were 23842.27 Pa and 218.81 K, the static pressure at fan face was 23842.27 Pa, and the nozzle total pressure, static pressure and total temperature were 35758.52 Pa 23842.27 Pa 703.39 K, respectively.

3.0   RESULTS

The critical regions to be considered in a CROR nacelle subjected to nonzero AoA are the inlet and cowl, which consist of areas where boundary-layer separation or shock waves can arise. Flow separation is prohibitive on both these zones, since it generates regions of reduced total pressure and velocity, which can substantially damage the counter-rotating propellers and the fan performance. Therefore, these are the areas of major interest for this work.

This section brings the flowfield results obtained with the CFD solver. The influence of different AoAs in the static pressure and Mach number contours around the nacelle are here evaluated. The total pressure at the fan, inlet and cowl surfaces are also presented. Moreover, the velocity vectors at the bottom region (BR) of the intake and at the top region (TR) of the cowl are analysed.

The Mach number and static pressure contours around the nacelle are shown respectively in Figure 6 and Figure 7. The total pressure at the fan, inlet and cowl surfaces are shown in Figure 8. Figure 9 shows the velocity vectors

coloured by Mach number on the lip BR and cowl TR, with the details of the boundary layer on the propeller entry region.

The contours for an AoA of 0° presented axisymmetric results, as expected, and the boundary layer was successfully captured, as can be seen in the low velocity region just above the cowl and midbody sufaces, in the Mach number contours. An increase in the Boundary layer thickness can be observed in the rear region of the forebody, for all the angles of attack, just in the propeller entry region.

As the angle of attack is increased, the Mach numbers in the front of the cowl BR tends to reduce, whilst a zone of high velocity is formed in the lip internal surface. For 6° and 8°, high velocities were attained, although always under subsonic conditions. For static pressure contours, a high pressure region is formed in the front of the cowl BR, whilst the pressure reduces in the lip zone.

(a) 0°

(b) 4°

(c) 6°

(d) 8°
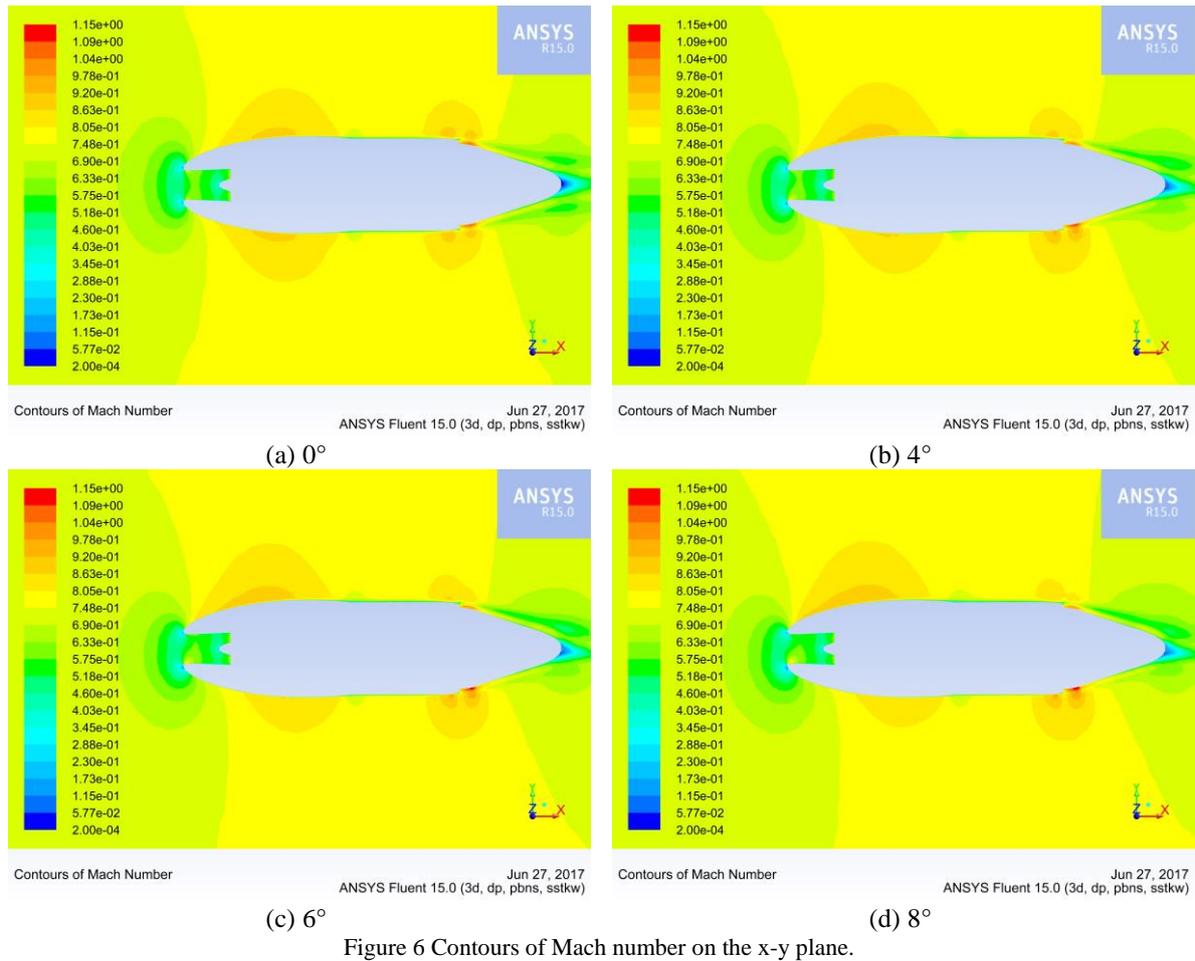
Figure 6 Contours of Mach number on the x-y plane.

(a) 0°

(b) 4°
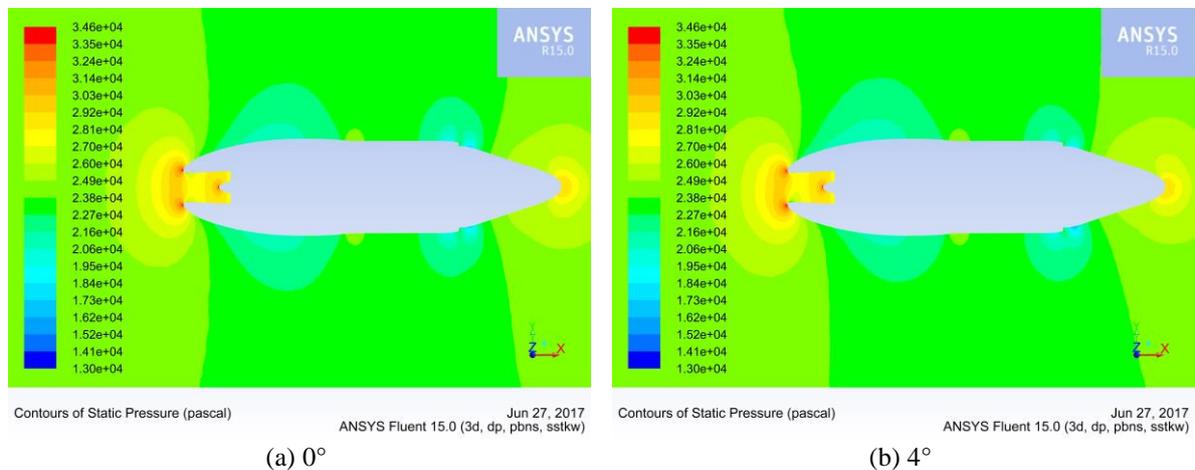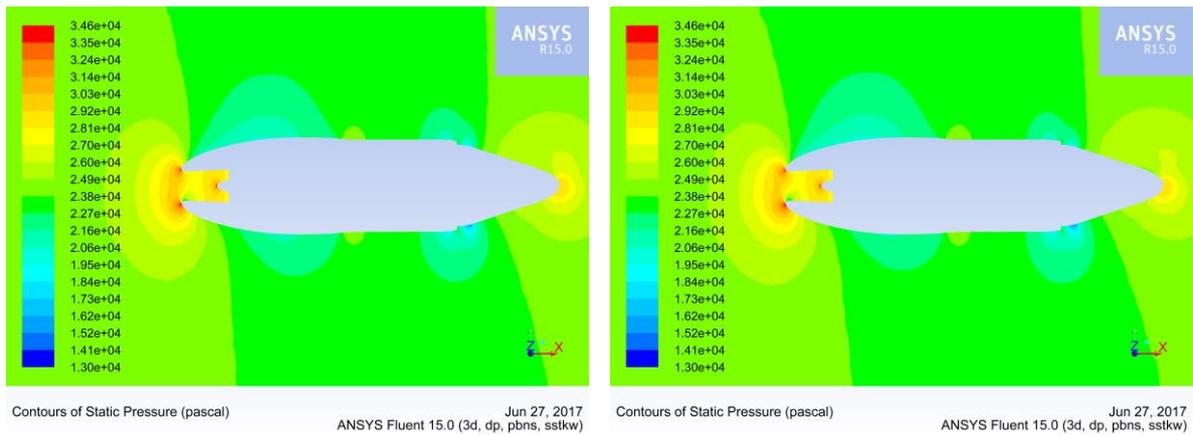
(c) 6°   (d) 8°

Figure 7 Contours of Static pressure on the x-y plane.
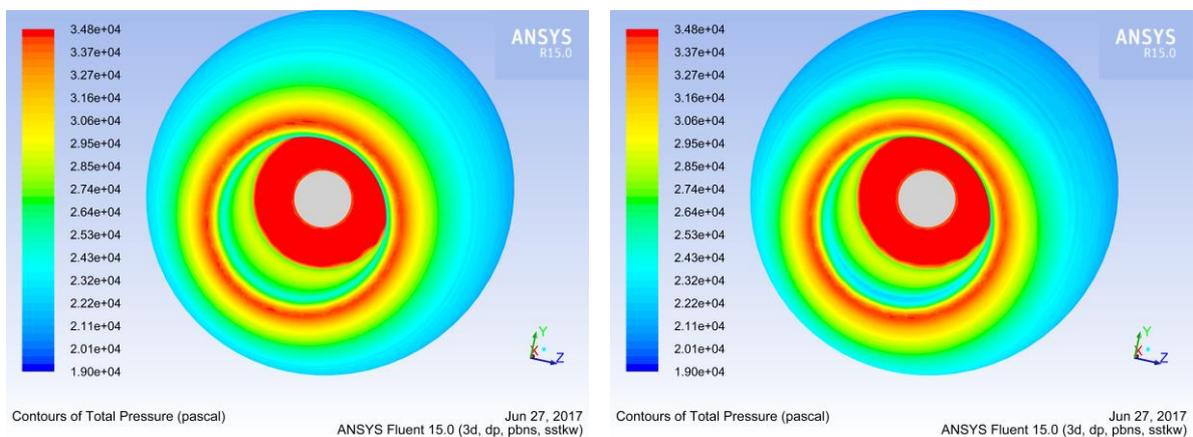
(a) 0°   (b) 4°
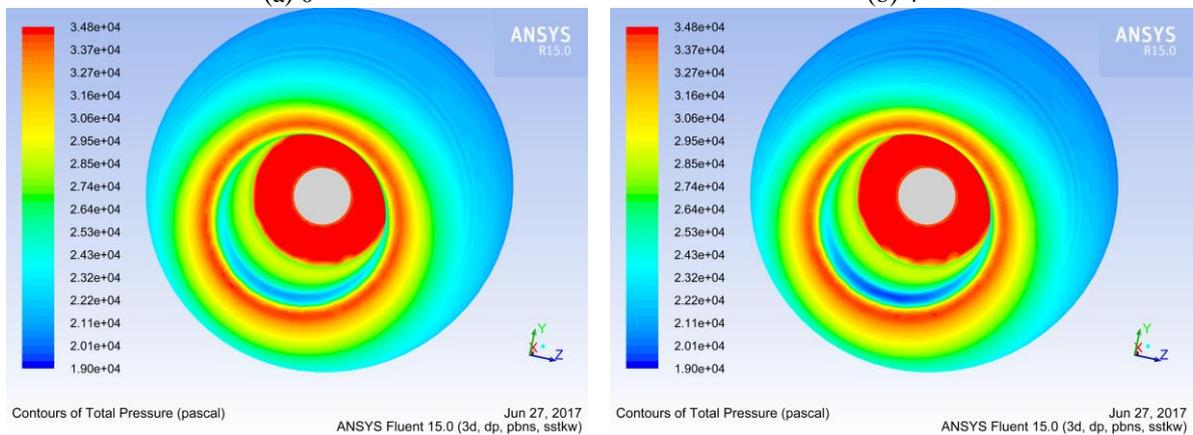
(c) 6°   (d) 8°

Figure 8 Contours of total pressure on the intake and fan surface.

By evaluating the Mach number contours, is possible to notice a boundary layer thickening in the upper region of the forebody and midbody, however no flow separation is observed. A slight boundary layer thickening also occurred in the lower region of the intake diffuser, which is confirmed by a small zone of total pressure reduction in the fan BR, for the AoAs of 6° and 8°. Iso-surfaces of zero axial velocity were created in the whole domain, to search for regions of recirculation in the inlet, although no flow distortion was noticed.

The velocity vectors have shown an appropriate smooth flow around the nacelle intake and cowl. The light boundary layer thickening, with the AoA increasing, can also be observed, in the low velocity regions. A detail of the vectors in the region of transition from forebody to midbody was captured, aiming at evaluating the boundary-layer in this region. Even for the higher AoA, the boundary layer has shown to be well attached, with no adverse pressure gradient evidence.

(a) 0°

(b) 4°

(c) 6°

(d) 8°
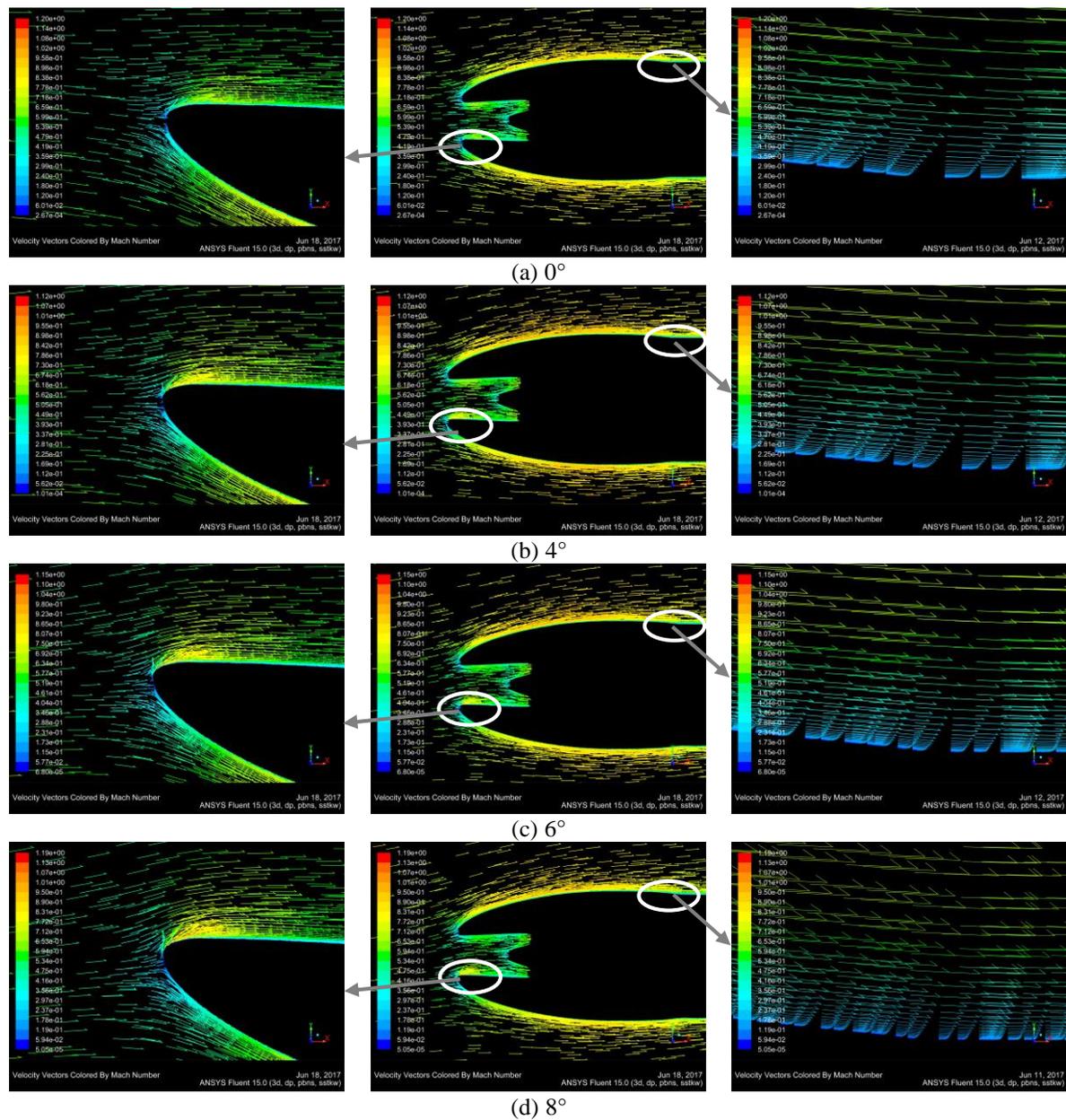
Figure 9 Velocity vectors on the nacelle lip and cowl.

4.0 CONCLUSIONS

A code for designing a CROR nacelle was created and an initial geometry was generated. The 3D flowfield around the proposed nacelle shape was evaluated for four angles of attack, simulating top of climb aircraft conditions. Although a slight boundary layer thickening was noticed in the TR of the cowl and in the BR of the inlet, with the increasing AoA, no flow separation was observed and hence the ingested boundary-layer won't perform substantial harm to the counter rotating propeller performance. High Mach number zones were detected in the lip BR, although with acceptable subsonic maximum values.

The implemented code was considered to be successful as a preliminary axisymmetric CROR nacelle geometry generator, in view of the results exposed in this paper. The next step of this research is to include the propellers in the nacelle midbody and evaluate their influence on the flowfield.